

Supplementary.

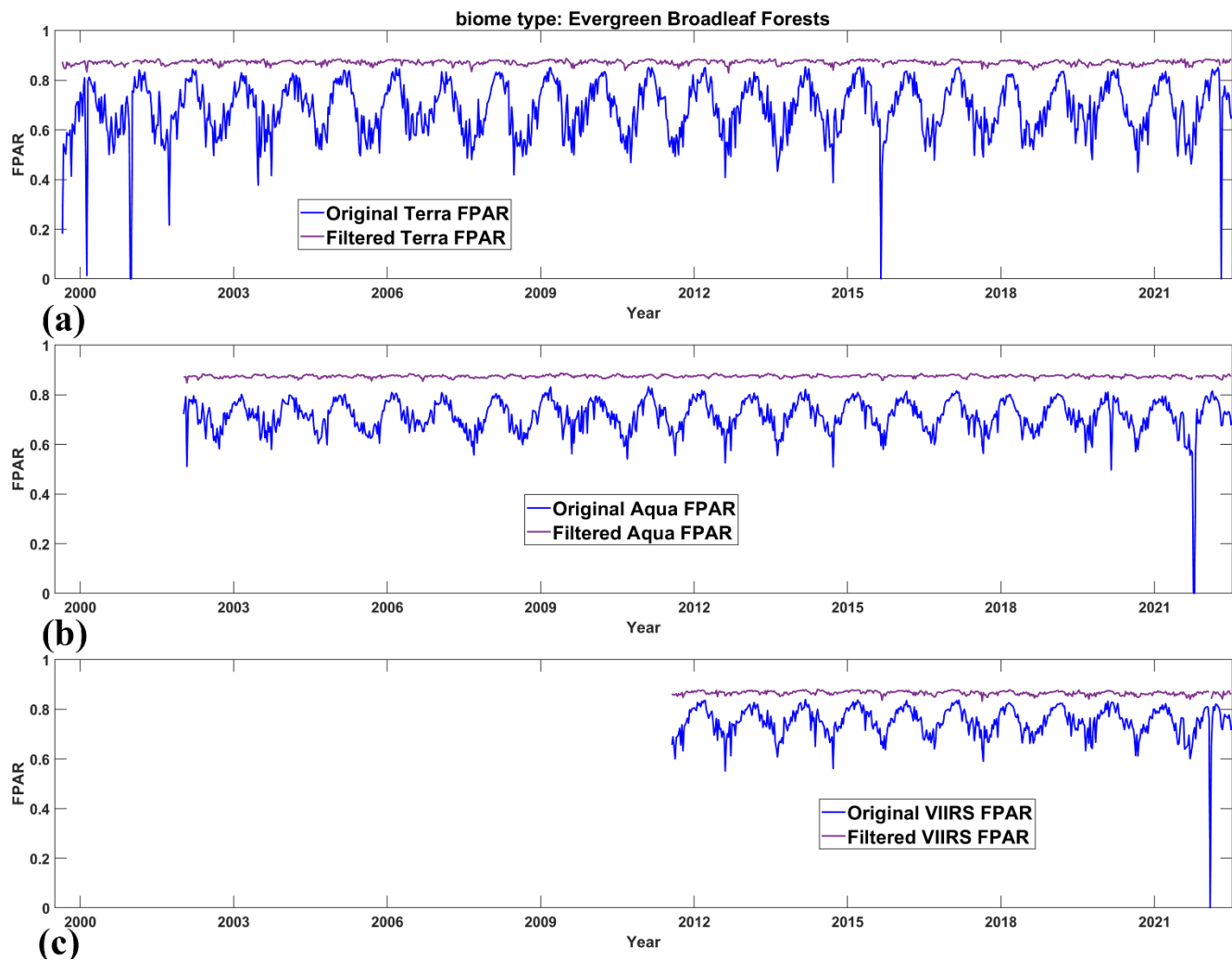
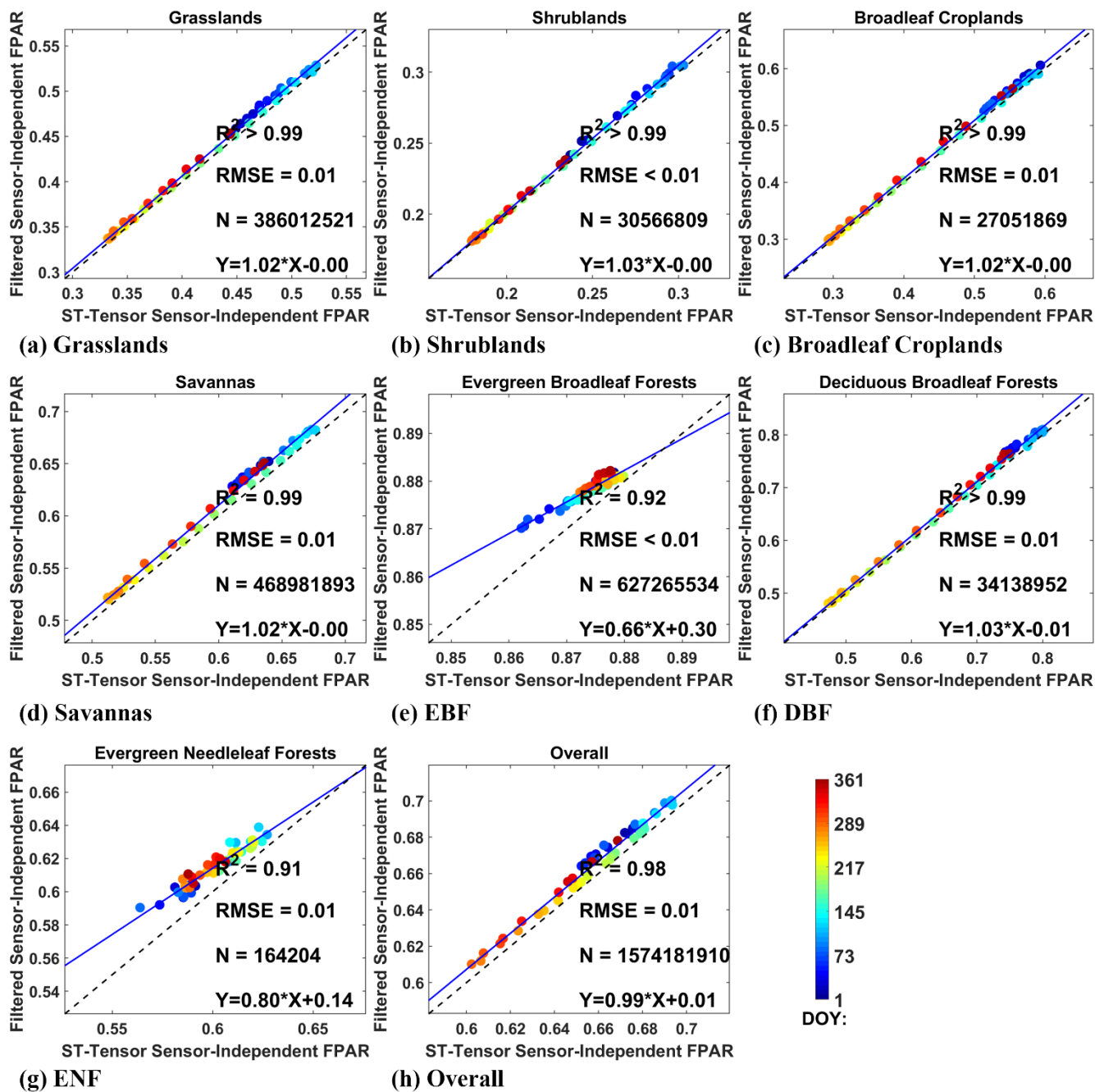


Figure S1. Same as Fig. 3 but for FPAR. The temporal comparisons between the original Terra/Aqua/VIIRS FPAR and Filtered Terra/Aqua/VIIRS FPAR for the EBF of Amazon Forest region.



5

Figure S2. Same as Fig. 6 but for FPAR. Comparisons of Filtered SI FPAR and ST-Tensor SI PARM 2000 to 2022 year for 5% pixels that Flag=1 in the selected Amazon Forest region (zoom-in case in Fig. 1).

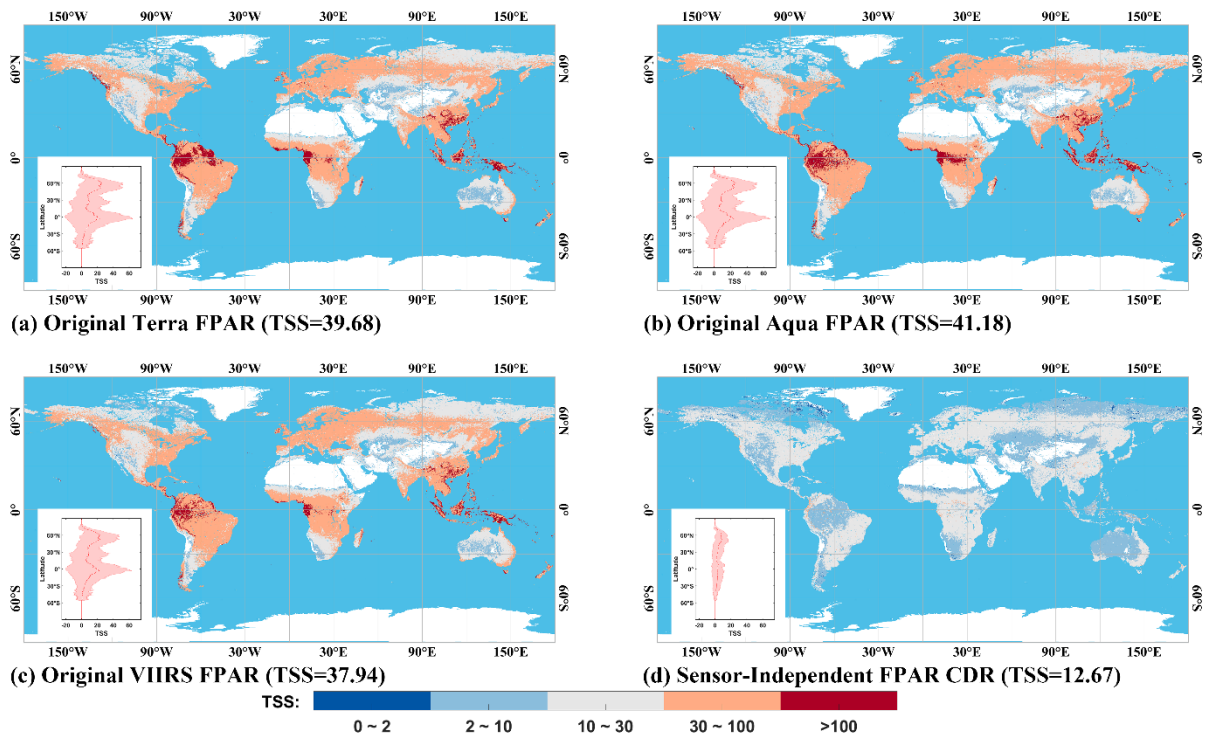


Figure S3. Same as Fig. 7 but for FPAR. The global distribution of FPAR TSS in each 0.05 degree \times 0.05 degree grid from 2013 to 2022.

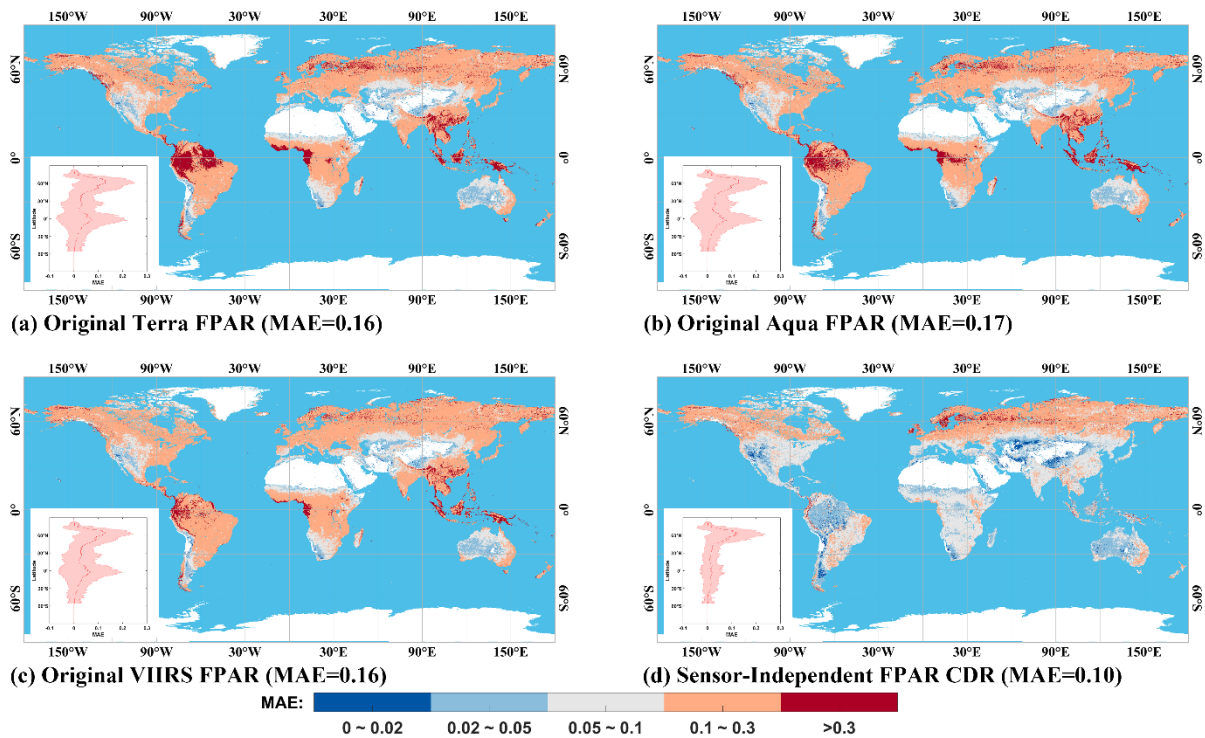


Figure S4. Same as Fig. 8 but for FPAR. The global distribution of FPAR MAE in each 0.05 degree \times 0.05 degree grid from 2013 to 2022.

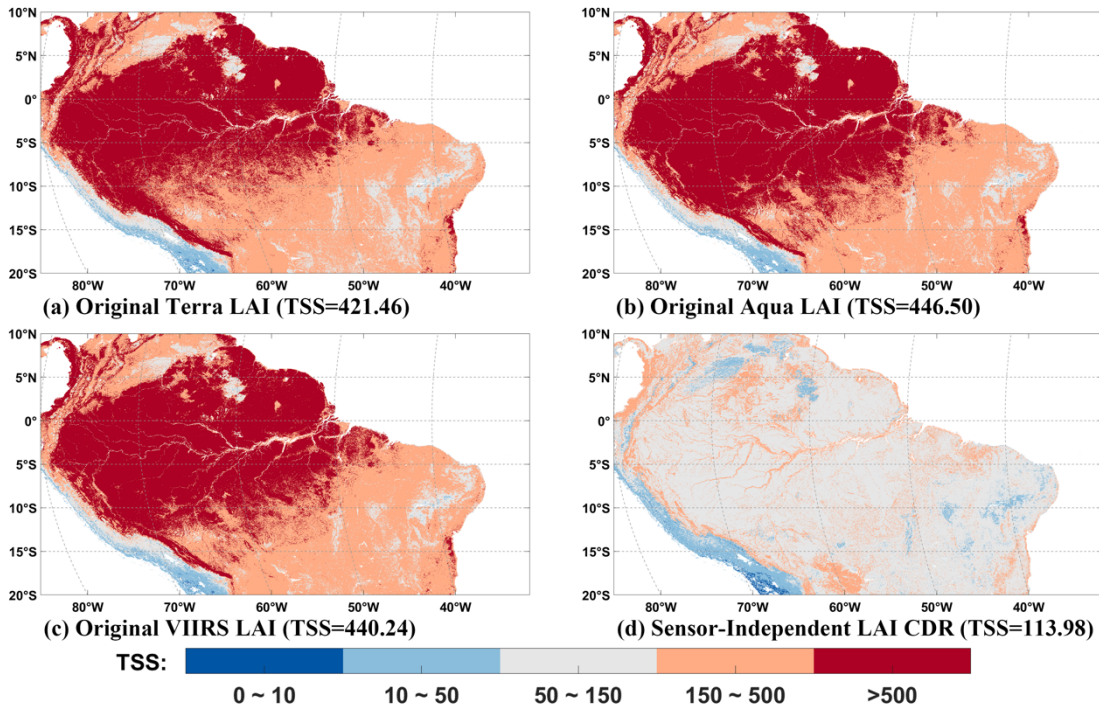
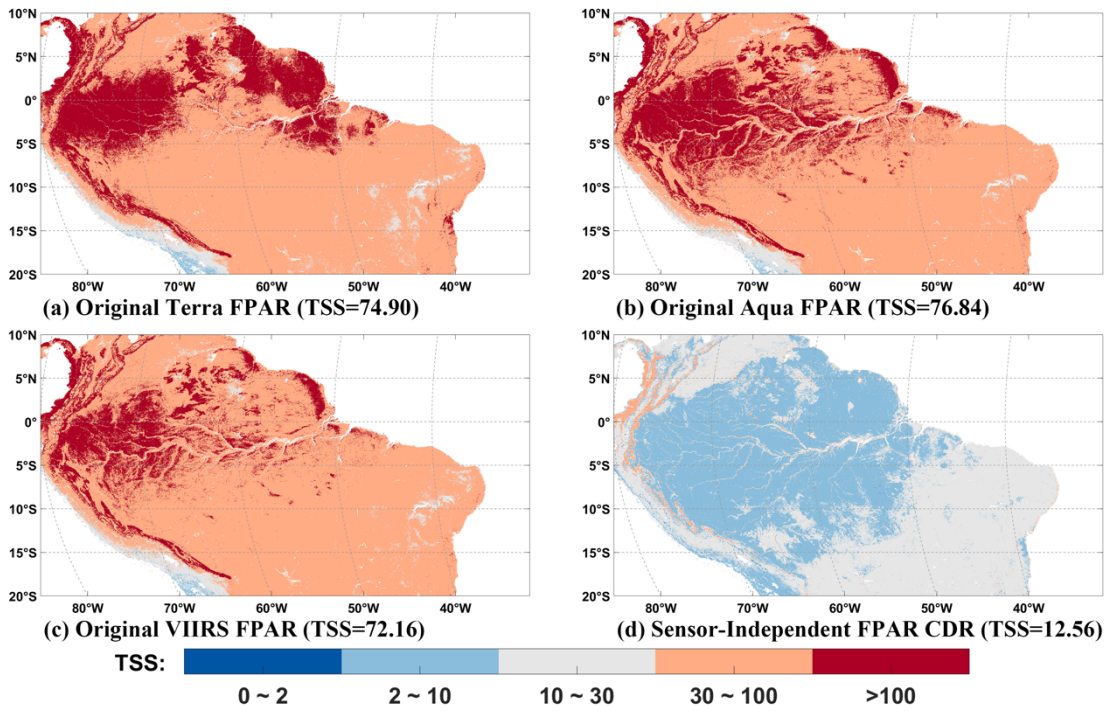
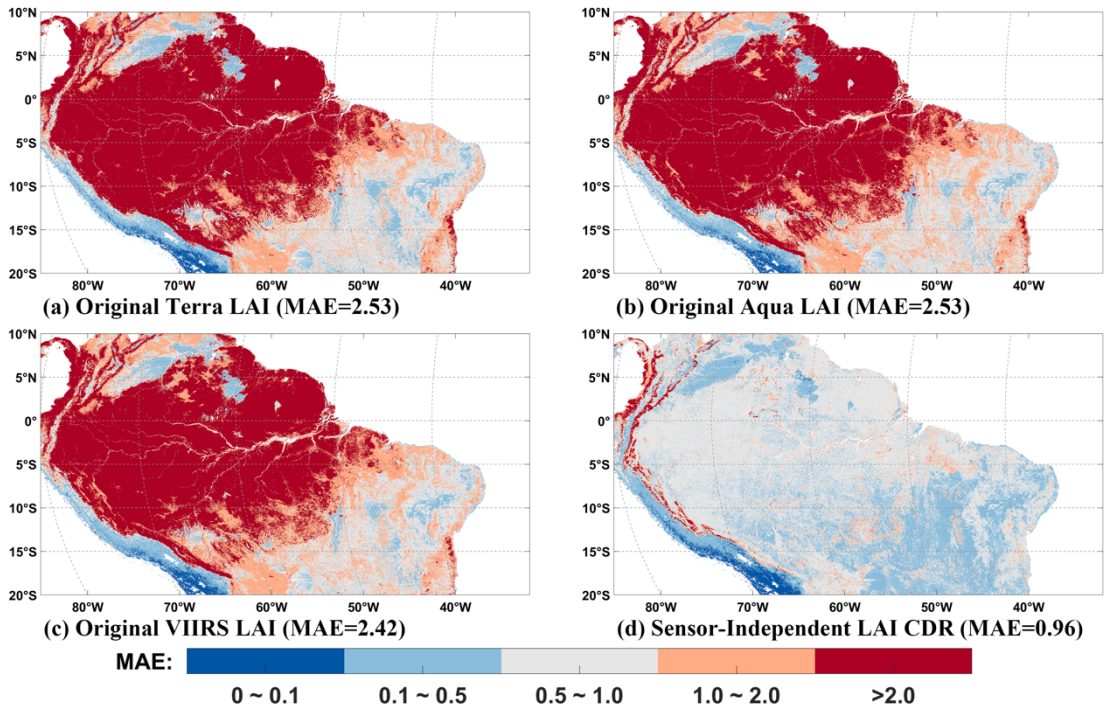


Figure S5. Same as Fig. 7 but for the Amazon Forest region. The spatial distribution of LAI TSS in each 500m \times 500m grid, with sinusoidal projection over the selected Amazon Forest region (zoom-in case in Fig. 1), from 2013 to 2022.



15

Figure S6. Same as Fig. S5 but for FPAR. The spatial distribution of FPAR TSS in each 500m x 500m grid, with sinusoidal projection over the selected Amazon Forest region (zoom-in case in Fig. 1), from 2013 to 2022.



20 **Figure S7.** Same as Fig. S5 but the metric is MAE. The spatial distribution of LAI MAE in each $500\text{m} \times 500\text{m}$ grid, with sinusoidal projection over the selected Amazon Forest region (zoom-in case in Fig. 1), from 2013 to 2022.

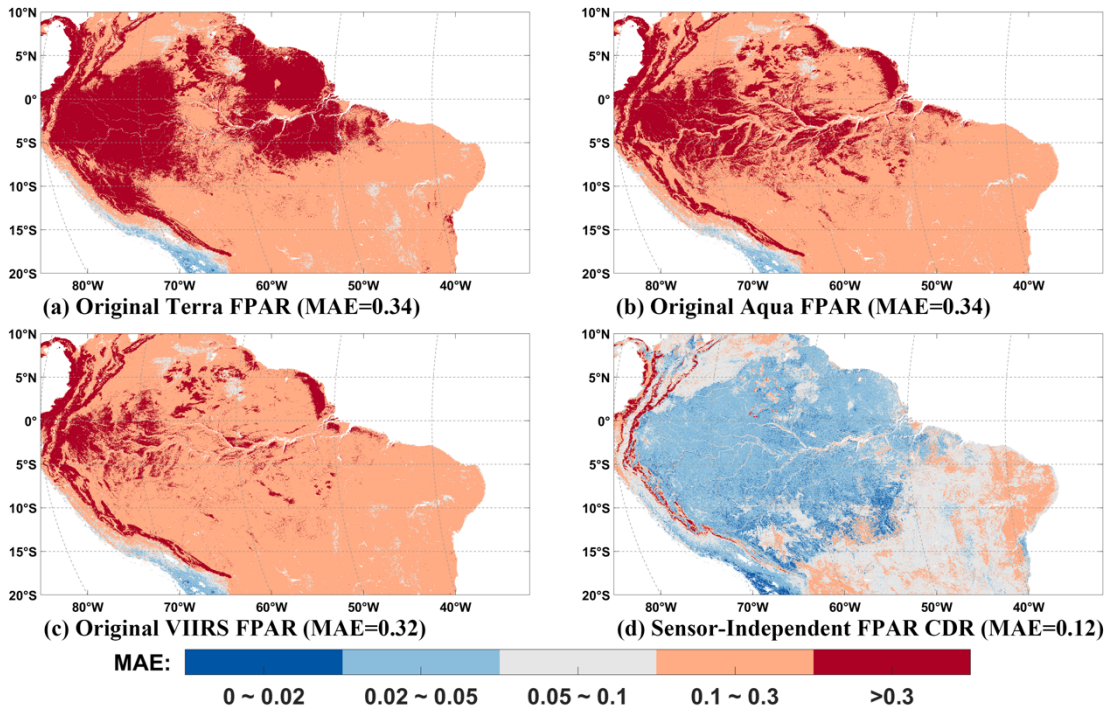
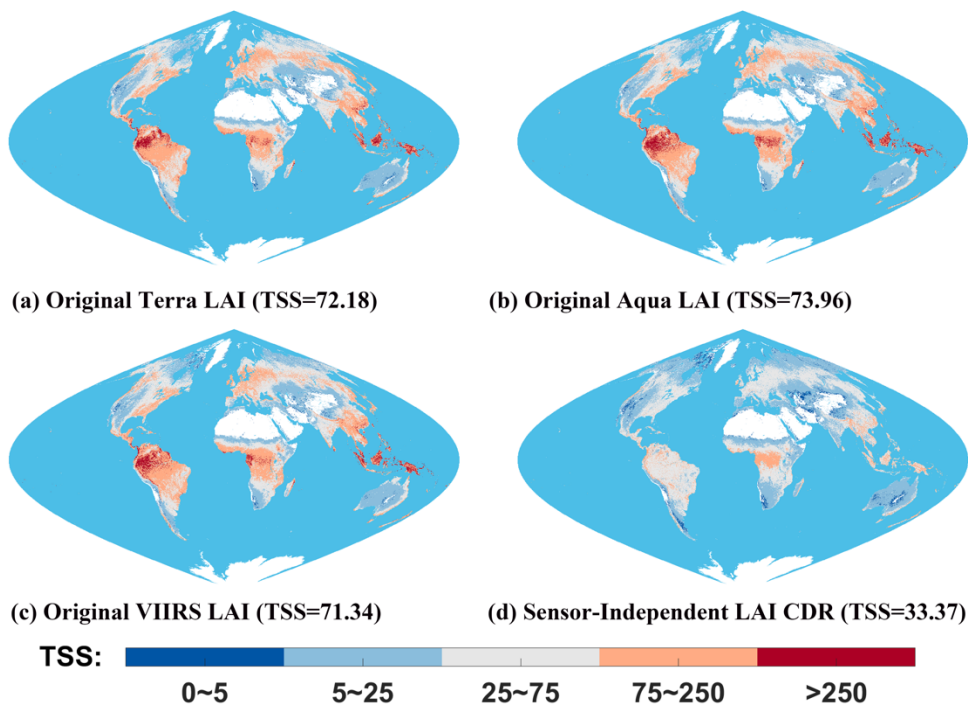


Figure S8. Same as Fig. S7 but for FPAR. The spatial distribution of FPAR MAE in each $500\text{m} \times 500\text{m}$ grid, with sinusoidal projection over the selected Amazon Forest region (zoom-in case in Fig. 1), from 2013 to 2022.



25 **Figure S9.** Same as Fig. S5 and the spatial resolution is 5km and the temporal resolution is bimonthly. The global distribution of LAI TSS in each 5km× 5km grid, with sinusoidal projection, from 2013 to 2022.

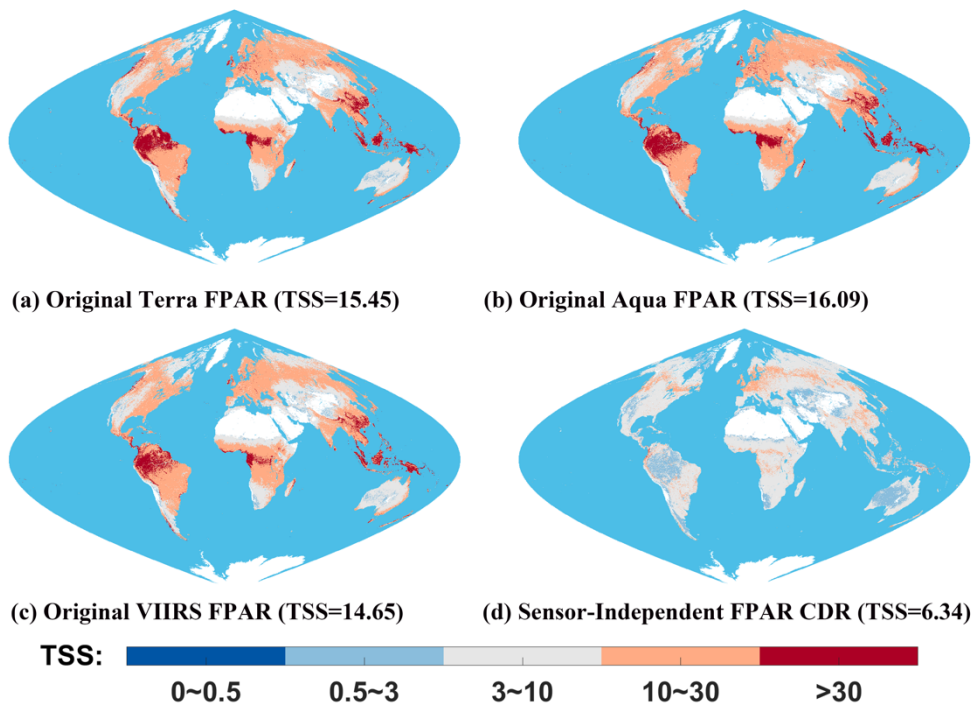
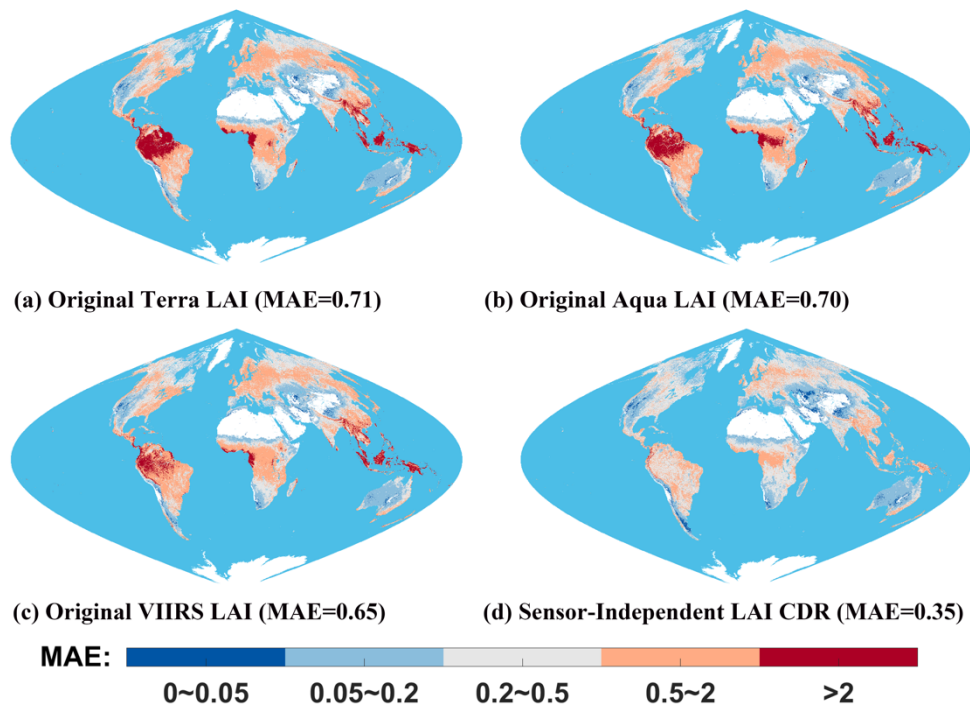
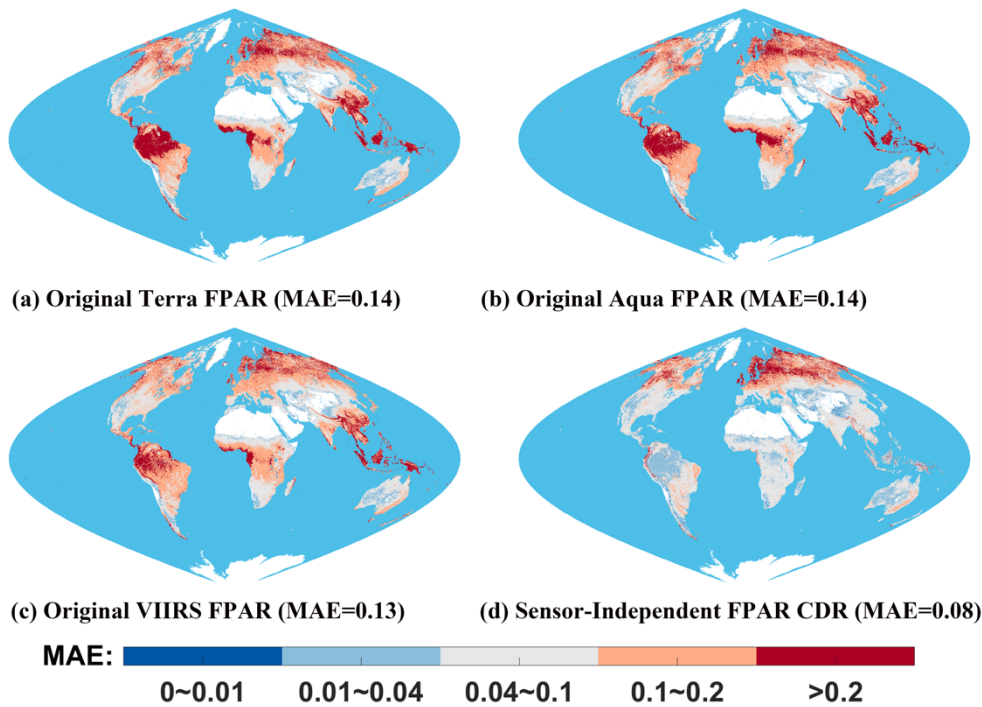


Figure S10. Same as Fig. S9 but for FPAR. The global distribution of FPAR TSS in each $5\text{km} \times 5\text{km}$ grid, with sinusoidal projection, from 2013 to 2022.



30

Figure S11. Same as Fig. S9 but the metric is MAE. The global distribution of LAI MAE in each $5\text{km} \times 5\text{km}$ grid, with sinusoidal projection, from 2013 to 2022.



35 **Figure S12.** Same as Fig. S11 but for FPAR. The global distribution of FPAR MAE in each 5km× 5km grid, with sinusoidal projection, from 2013 to 2022.

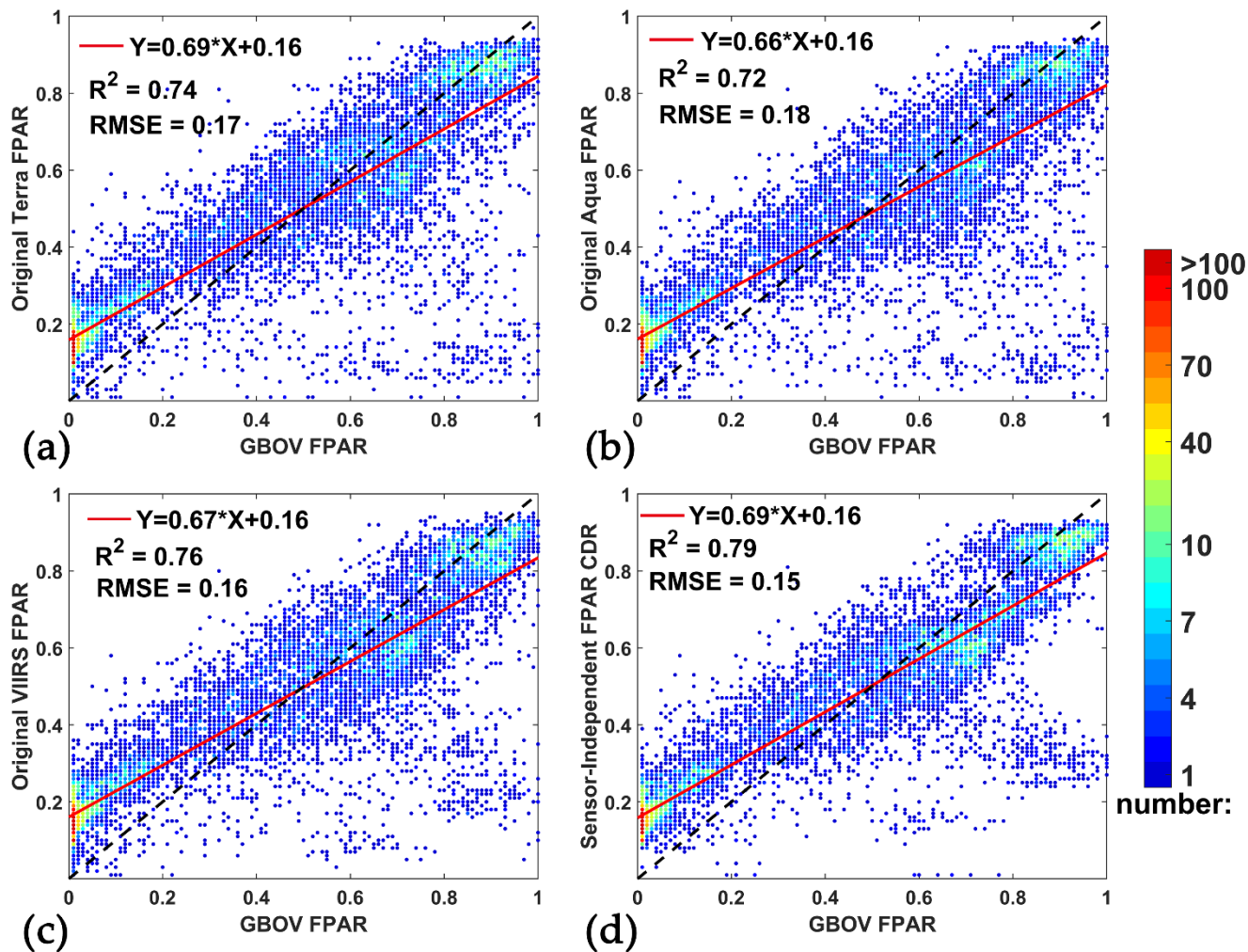
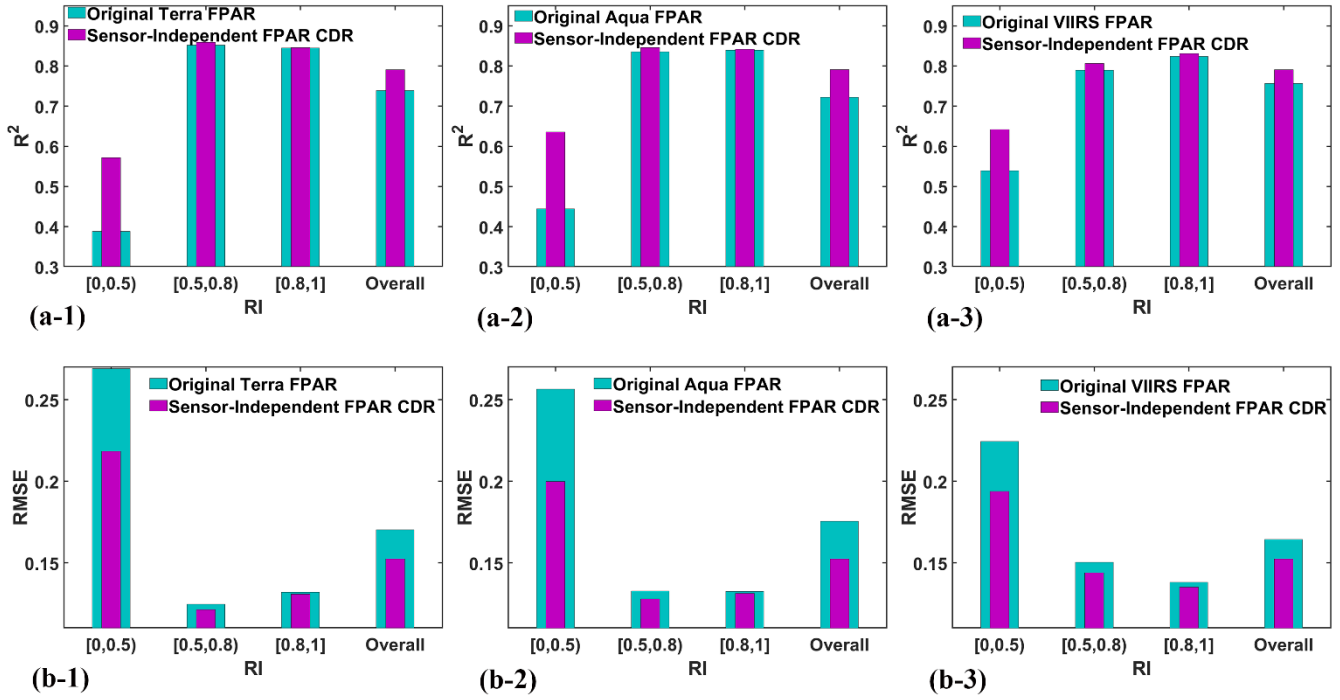


Figure S13. Same as Fig. 9 but for FPAR. Comparisons of original Terra/Aqua/VIIRS FPAR and SI FPAR CDR with ground GBOV FPAR.



40 **Figure S14.** Same as Fig. 10 but for FPAR. The R^2 and RMSE between original Terra/Aqua/VIIRS FPAR and SI FPAR CDR and GBOV FPAR in different RI ranges.

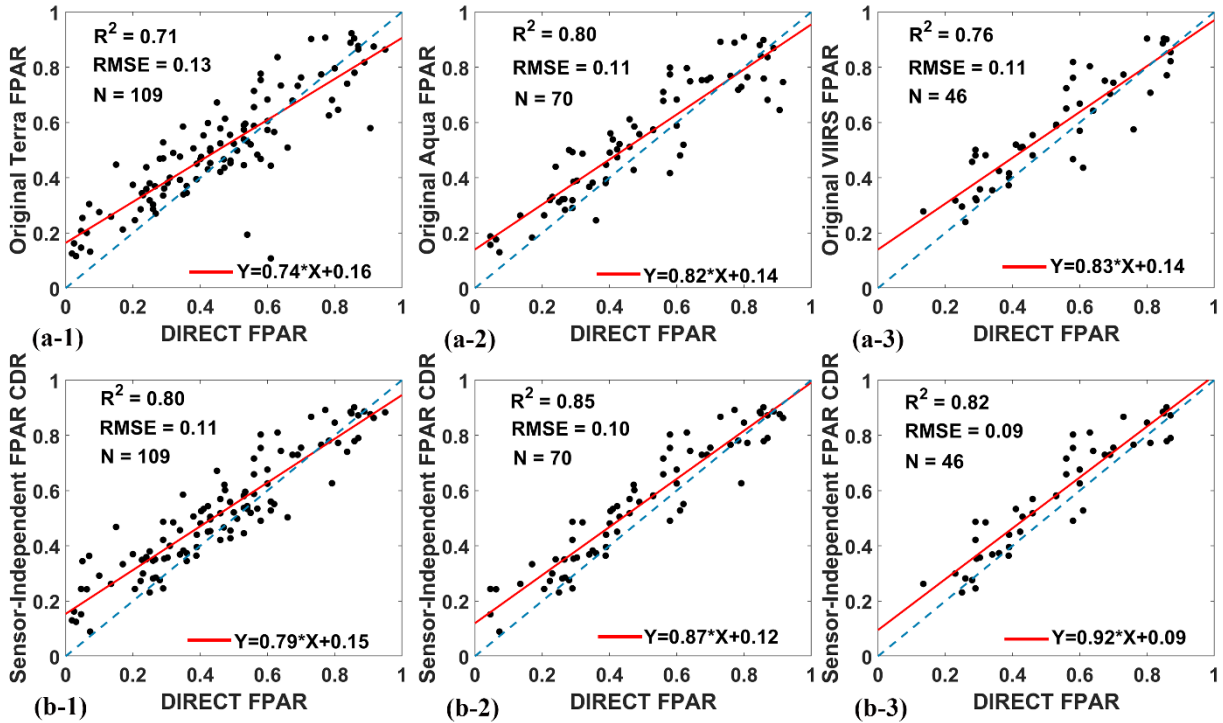


Figure S15. Same as Fig. 11 but for FPAR. Comparisons of original Terra/Aqua/VIIRS FPAR and SI FPAR CDR with ground DIRECT2.1 FPAR measurements.